Interannual (ENSO) and Interdecadal (ENSO-like) Variability in the Southern Hemisphere Tropospheric Circulation*

RENÉ D. GARREAUD AND DAVID S. BATTISTI

Department of Atmospheric Sciences, University of Washington, Seattle, Washington

5 May 1998 and 30 July 1988

ABSTRACT

Recent work has identified variability in the Pacific Ocean SST with a structure qualitatively similar to ENSO, but at lower frequencies than ENSO. Zhang et al. have documented the atmospheric circulation anomalies in the Tropics and Northern Hemisphere that are associated with decadal ENSO-like variability and compared these anomalies to those associated with the (interannual) ENSO cycle.

Here the authors extend the study of Zhang et al. to the Southern Hemisphere using the National Centers for Environmental Prediction–National Center for Atmospheric Research reanalysis data for 1958–96. Consistent with previous studies, the Southern Hemisphere circulation anomalies associated with ENSO display a teleconnection pattern from the central tropical Pacific into the far southeastern Pacific Ocean. Comparatively larger circulation anomalies are found in the Southern Hemisphere associated with the decadal ENSO-like variability, though aloft the structure of the anomalies emphasizes the polar vortex with an adorning wavenumber-3 anomaly along 60°S. There is a common pattern of SST anomalies throughout the South Pacific associated with the ENSO and the decadal ENSO-like variability, and these anomalies appear to be forced by (inferred) surface heat flux anomalies that should be associated with the changes in the atmospheric circulation. Finally, subtle differences in the tropical circulation anomalies are found to be associated with the two different timescales of variability. Further studies are required to demonstrate whether these differences are responsible for the different structure of the tropospheric mid- and high-latitude circulation anomalies in the Northern and Southern Hemispheres.

1. Introduction

Analyses of the structure of the ocean–atmosphere variability in the Southern Hemisphere have been hampered by the paucity of meteorological and oceanographic data, especially over the southern oceans. While many studies over the last two decades have documented the structure of the interannual variability of the tropospheric circulation (largely dominated by ENSO) in the Tropics (e.g., Wallace et al. 1998, and references therein) and Northern Hemisphere (NH; e.g., Horel and Wallace 1981), fewer works have addressed the year-to-year circulation anomalies in the Southern Hemisphere (SH; e.g., Rogers and van Loon 1982; van Loon and Shea 1987; Karoly 1989; Kiladis 1997). Recent work has also focused on interdecadal climate variability of the ocean–atmosphere over the North Pacific and parts of North America (e.g., Nitta and Yamada

1989; Trenberth 1990; Trenberth and Hurrel 1994; Nakamura and Yamagata 1997), in which the broadly known "regime shift" of 1976–77 appears as an outstanding example (e.g., Graham 1994).

Zhang et al. (1997), hereafter referred as ZWB, documented the spatial signatures of the interdecadal climate variability in the Pacific basin and compared them with the patterns associated with the ENSO cycle. Their analysis is largely based on marine surface observations from the Comprehensive Ocean–Atmosphere Data Set (COADS; Fletcher et al. 1983) for the period 1950–93 and restricted to the region north of 30°S. They found that interannual and interdecadal variability exhibit roughly similar spatial signatures in the sea surface temperature (SST), sea level pressure (SLP), and wind stress fields. The recently released reanalyzed atmospheric fields by the National Centers for Environmental Prediction–National Center for Atmospheric Research (NCEP–NCAR) encompassing the period from 1958 to 1996 in a 2.5° × 2.5° lat–long global grid (Kalnay et al. 1996) enable us to reexamine the structure of the low-frequency variability of the atmosphere and extend the results of ZWB to focus on features in the SH south of 30°S. In this short contribution we have followed the same methodology of ZWB. The leading EOFs of the SST that capture most of the interannual (ENSO-related)

Corresponding author address: Dr. René D. Garreaud, Department of Geophysics, University of Chile, Casilla 2777, Santiago, Chile.
E-mail: rgarreau@dgf.uchile.cl

and interdecadal (ENSO-like) components are regressed on relevant meteorological fields, to reveal some of their spatial signatures.

As described in detail in Kalnay et al. (1996), the 6-hourly reanalyzed fields were produced using a frozen weather prediction model and an enhanced observational database that includes conventional, aircraft, and satellite data, and hence they represent one of the most complete, physically consistent datasets of the atmospheric circulation and related thermodynamic fields. However, before presenting our results, it is worth commenting on some important caveats in the use of the NCEP–NCAR reanalysis. The model uses prescribed SST and sea ice as lower boundary conditions. The SST boundary condition is the Reynolds reanalysis (Reynolds and Smith 1994) from 1982 onward; the U.K. Meteorological Office SST dataset (Folland and Parker 1995) was used for the early period. Since SST observations south of 30°S are particularly sparse (Folland and Parker 1995), the extrapolated SST field in this region is largely determined by the algorithm used in its calculation, rather than representing an accurate picture of the actual SST field. Before 1973 the sea ice dataset used in the NCEP–NCAR reanalysis project undergoes a climatological mean annual cycle in the Southern Hemisphere (Parker et al. 1995; Kalnay et al. 1996), despite the significant year-to-year variability of the sea ice around Antarctica (e.g., Simmonds and Jacka 1995). Hence, the reanalyzed air temperature field near the ice edge is heavily influenced by the lack of sea ice anomalies in the surface boundary conditions. The third caveat in the use of the NCEP–NCAR reanalysis for studies over the Southern Hemisphere involves incorrectly assimilated Australian surface pressure bogus data (PAOBs) between 1979 and 1992. Although this error must be kept in mind in the foregoing discussion, the assessment by NCEP–NCAR (see http://wesley.wwb.noaa.gov/paobs/) indicates that the impact of this mislocation is very small on monthly and longer timescales.

2. Results

Figure 1 shows the time series of the 6-yr high-pass filtered cold tongue index (CT*) and the ''residual'' time series of the global leading EOF of SST (GR) for the period 1958–93. The cold tongue index (CT) is the average of SST anomaly in the equatorial Pacific (6°N–6°S, 180°–90°W), and it captures most of the ENSO-related variability (Deser and Wallace 1990). Although most of the variance of CT is contained in the interannual range (~2–6 years), we applied a 6-yr high-pass filter to CT to exclude interdecadal variability in the resulting time series (CT*). ZWB performed an EOF analysis on the global monthly anomalies of SST. The corresponding principal component (G) is still dominated by interannual variability but also exhibits longer period variability. The CT* was linearly fitted to G, and
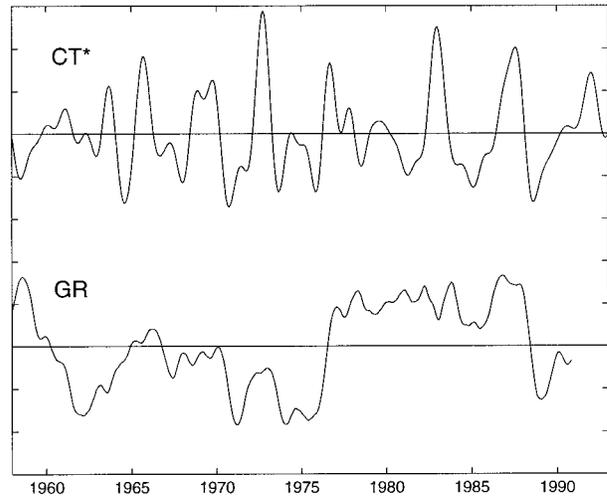

FIG. 1. Normalized time series of the 6-yr high-pass filtered cold tongue index (CT*) and global residual (GR). The interval between tick marks is 1.0 std dev.

the resulting time series was substracted from G to form the global residual time series (GR) shown in Fig. 1. Although GR also contains some year-to-year variability, it is linearly independent of CT*, and it captures most of the interdecadal variability of the global SST (ZWB).

a. Interannual variability

The regression of SST, wind at the 0.995 sigma level (hereafter referred as surface wind), and SLP onto CT* using all calendar months is shown in Fig. 2 and can be compared with Fig. 12 of ZWB. The signatures of the interannual variability on the SST field in the SH are mostly confined to the Pacific basin. As hinted in the ZWB analysis (their Fig. 12a), the subtropical South Pacific is dominated by anomalies out of phase with the ones occurring in the tropical Pacific, centered at about 30°S, forming a symmetric pattern about the equator with their counterpart in the North Pacific. Farther south, the SST–CT* regression changes its sign, to reach a maximum over the Ross Sea. The consistency of these features in the SST field with the atmospheric circulation above is discussed later. The spatial structure of the interannual variability of the SLP field (Fig. 2c) in low latitudes is characterized by the well-known dipole over the southern Pacific and parts of the Indian Ocean, which lies in the heart of the Southern Oscillation. The region of negative CT*–SLP regressions over the central subtropical Pacific extends southwestward to reach the Southern Ocean below Australia.

The ENSO-related SLP pattern in the midlatitudes is largely dominated by a region of positive values centered at 60°S over the southeast Pacific (Fig. 2c). The equivalent barotropic character of this feature is evident
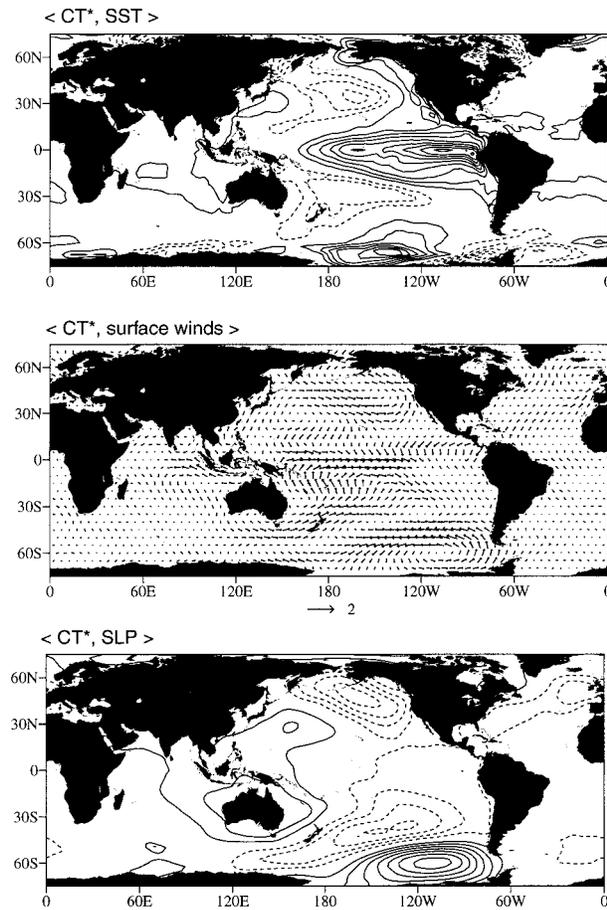
FIG. 2. Global reanalyzed fields regressed upon CT*. (top) Sea surface temperature (SST). Contour interval is 0.1 K per standard deviation of CT* (std dev)$^{-1}$. The zero contour is omitted and negative contours are dashed. (middle) Surface winds. The reference vector is 1.5 m s^{-1} (std dev)$^{-1}$. (bottom) Sea level pressure (SLP). Contour interval is 0.25 hPa (std dev)$^{-1}$. The zero contour is omitted and negative contours are dashed. Regressions are based on all calendar months, from Jan 1958 to Dec 1993.

in the regression of CT* upon geopotential height at 250, 500, and 1000 hPa for the winter months (Figs. 3a–c). At the upper levels, there is a signature of a wave train extending from the low latitudes near the date line toward the southeast Pacific. The so-called Pacific–South America pattern (PSA; Mo and Higgins 1998) is consistent with the Rossby wave response to equatorial anomalous heating (Hoskins and Karoly 1981) and it resembles the Pacific–North America (PNA) pattern over the NH (Wallace and Gutzler 1981). This wintertime, wavelike pattern was found by Karoly (1989) in his composite analysis of three ENSO events (1972, 1976/77, and 1982), and it also emerges as one of the leading circulation pattern in the SH in timescales ranging from daily (Mo and Ghil 1987), to intraseasonal (Mo and Higgins 1998), to interannual (Kidson 1988). The presence of a deep, anticyclonic anomaly over the

southeast Pacific during the warm phase of ENSO is consistent with an increasing number of blocking episodes to the west of the southern tip of South America and Antarctica peninsula during ENSO, reported by Rutllant and Fuenzalida (1991) and Renwick (1998). The blocking of the westerly flow in conjunction with the weakening of the South Pacific subtropical high indicates that there is an equatorward shift of the storm track axis over the central Pacific from its climatological position (Sinclair et al. 1997) and, consequently, the wintertime precipitation tends to be higher than normal across subtropical South America during the warm phase of ENSO, while at the same time the southern tip of the continent experiences drier than normal conditions (e.g., Aceituno 1988).

The maps in Figs. 3a–c also show two minor negative centers around 60°S, one over the Weddell sea and the other at 110°E, and a weaker but extensive belt of positive values centered at 40°S extending eastward from the eastern Atlantic to Australasian sector. This midlatitude belt of anticyclonic anomalies across most of the Indian Ocean (for CT* > 0) may be connected with the decreasing number of cyclones in the subtropical Indian Ocean, Australia, and the southwest Pacific during the warm phase of ENSO (Sinclair et al. 1997), which produces drier than normal conditions in this region (e.g., Ropelewski and Halpert 1996).

The annual march of the midlatitude circulation anomalies associated with ENSO variability is illustrated in Fig. 4 (left panels) by the seasonal regression maps between 500-hPa geopotential height and CT*. The midtropospheric PSA pattern is weaker during the austral summer (December–February; DJF) and strongest in the autumn. While the trough over the subtropical Pacific reaches its maximum extent in July–August (JJA) the positive anomalies in the far southeast Pacific are somewhat less pronounced in midwinter relative to the anomalies in the transition seasons. This result is consistent with the composite analysis of Kiladis (1997), where it is found that the pressure anomaly pattern during cold phase Southern Oscillation events is mostly the opposite to those during warm events, except during the JJA, when the ''inverse PSA'' is not very evident. The wintertime lack of symmetry between cold and warm phases of the Southern Oscillation would produce a weaker signal in a linear analysis as the one presented here.

The surface winds regressed upon CT* (Fig. 2b) exhibit tropical and NH features consistent with those obtained by ZWB using COADS-derived surface wind stress and CT*. In the SH midlatitudes, most of the amplitude is concentrated over the southeast Pacific, in association with the prominent center of SLP anomalies. For instance, during the warm phase of the ENSO cycle, there is a significant decrease of the westerlies in the equatorward flank of the southeast Pacific anticyclonic anomaly. The weakening of the air–sea fluxes and the warm air advection by the
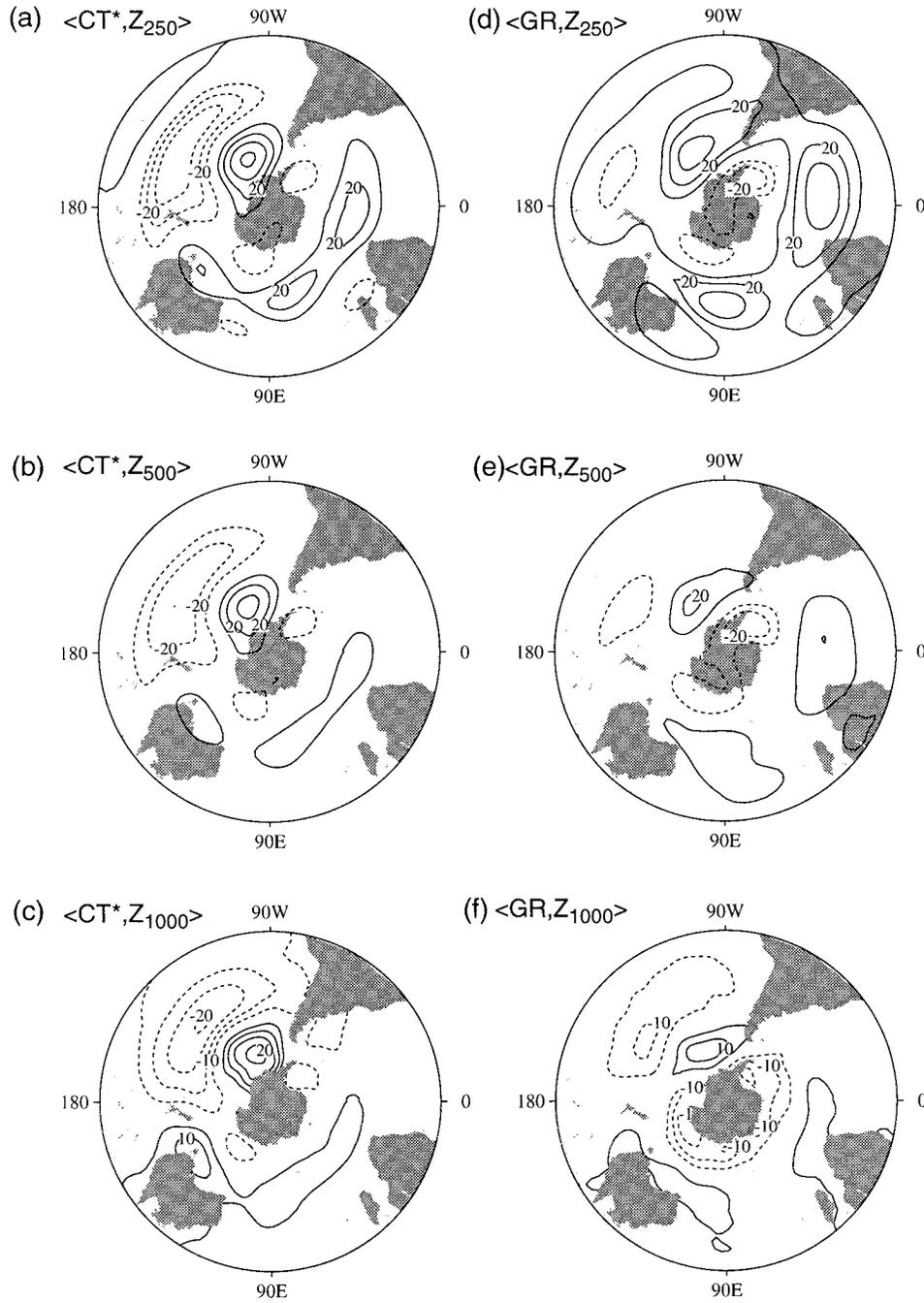
FIG. 3. Jun–Aug monthly mean values of geopotential height regressed upon (left) CT* and (right) GR. The levels are (a), (d) 250 hPa [contour interval is 10 m (std dev)$^{-1}$]; (b), (e) 500 hPa [contour interval is 10 m (std dev)$^{-1}$]; and (c), (f) 1000 hPa [contour interval is 5 m (std dev)$^{-1}$]. The zero contour is omitted and negative contours are dashed.

northerly flow would tend to increase the SST at mid- and high latitudes between 180° and 120°W, which is consistent with the positive regression coefficient of the (extrapolated) SST upon CT* shown in Fig. 2a. The opposite situation prevails to the east of the southeast Pacific anticyclone where a tongue of cold water extends from the Bellingshausen Sea into the southwest Atlantic (for CT* > 0). Over the Southern Ocean south of Australia there is a belt of increasing westerlies that turns equatorward near New Zealand and increases the low-level convergence in the South Pacific convergence zone.
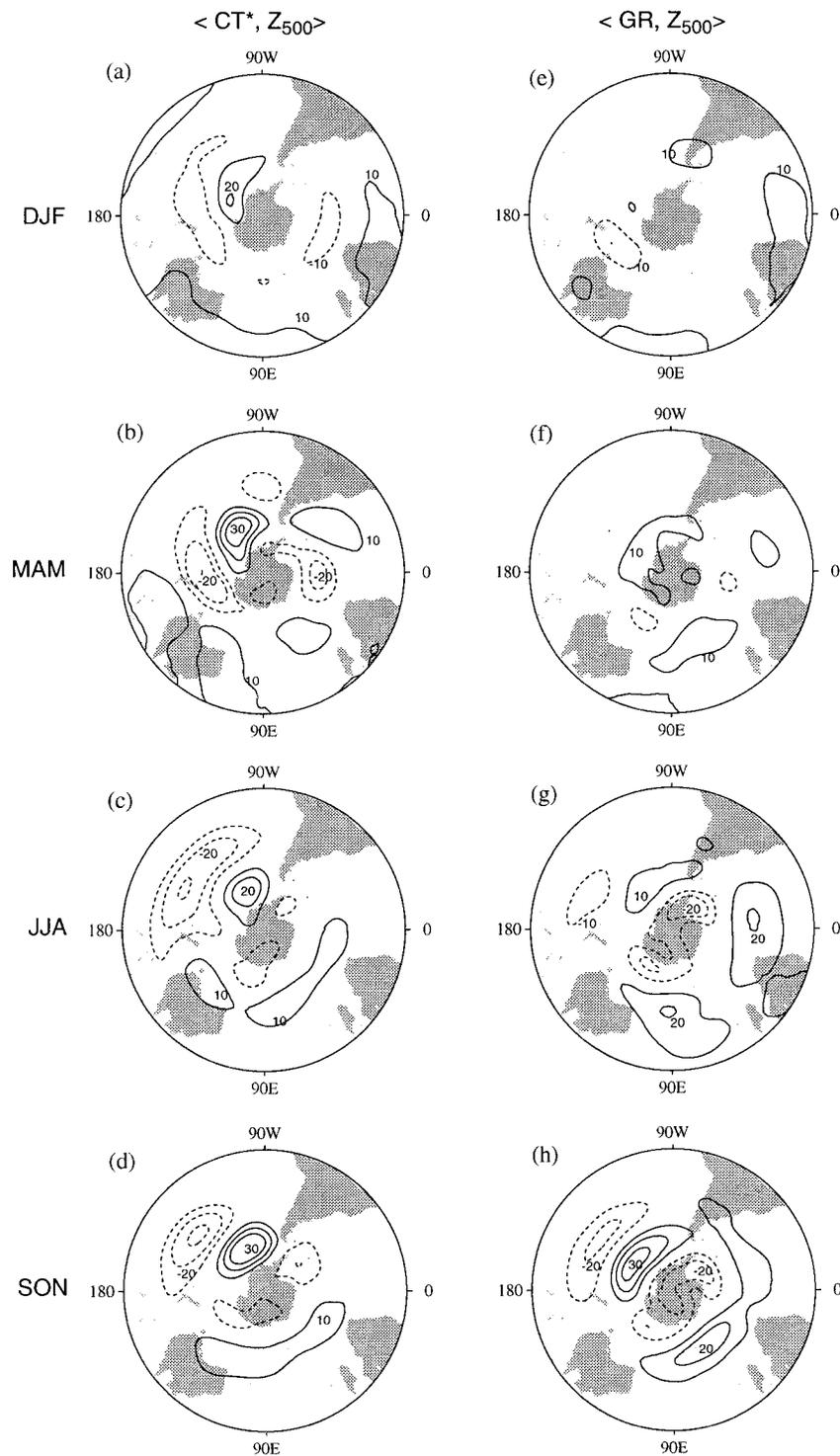
FIG. 4. Seasonally averaged 500-hPa geopotential height regressed upon (left) CT* and (right) GR for each season (indicated in the left side of the figure). Contour interval is 10 m (std dev)$^{-1}$, negative values are dashed, and the zero contour is omitted.
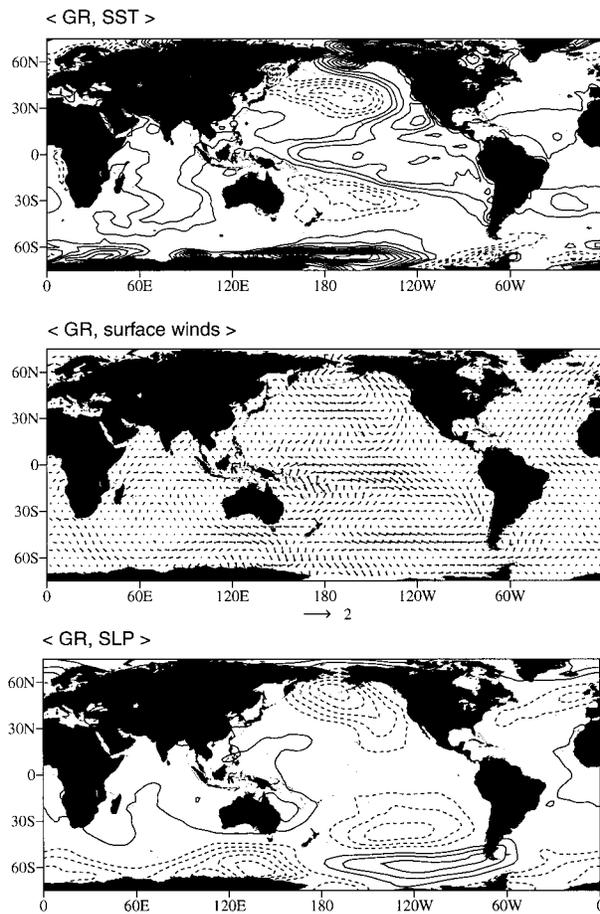
FIG. 5. As in Fig. 2, but based on GR.

b. Interdecadal variability

As pointed out by ZWB, the dominant spatial signatures of SST, SLP, and wind stress associated with interdecadal variability may be described as ENSO-like. Over the SH sector that was not shown in ZWB, the SLP field regressed upon GR (Fig. 5c) indeed reveals features similar to its interannual counterpart (Fig. 2c), most notably the presence of a region of positive anomalies over the far southeast Pacific with a barotropic structure in the vertical (Figs. 3d–f), and a broad region of negative regressions over the central South Pacific. They indicate, for instance, the presence of higher SLP in the southeast Pacific and lower SLP across much of the subtropical Pacific from 1977 onwards. The signature of interdecadal variability on the SST field (Fig. 5a) is also qualitatively similar to the obtained in the interannual case (Fig. 2a). However, the regression near Antarctica between 180° and 120°W seems suspiciously high.

There are also some noteworthy differences between the spatial signatures of the interannual and interdecadal variability, which are more clear in the maps of wintertime geopotential height at several levels regressed upon GR shown in Fig. 3. In particular, the interdecadal signature in the geopotential height centered over the far southeast Pacific is weaker and more zonally elongated, extending from the date line to the southern tip of South America. Also in the decadal pattern, the subtropical cyclonic anomaly over the central Pacific is weak and decreases with height and toward the equator, and the signature of an upper-level wave train from the tropical Pacific near the date line to the southeast Pacific is barely discernible in the upper-level geopotential height field regressed upon GR (Figs. 3c and 3d). The opposite situation prevails in the NH, where the PNA pattern is more clearly defined in the interdecadal variability than in the interannual variability (e.g., Fig. 13 of ZWB).

The feature in the GR–geopotential height regressions over and around Antarctica (roughly poleward of 60°S) is more pronounced than its interannual counterpart (cf. Figs. 3c, 3f). The SLP and geopotential height regression patterns exhibit a belt around Antarctica, with the exception of the southeast Pacific side and two closed centers at 145°E and 50°W with amplitudes as large as the ones found in the southeast Pacific region. In the middle and upper troposphere (Figs. 3d,e; 4e–h), the region of negative regressions covers most of the continent, forming an elongated quasi-polar vortex. Over the midlatitude Southern Oceans (~45°S) the geopotential height anomalies tend to be out of phase with those at higher latitudes and amplify from the lower to the upper troposphere. Hence, the spatial signature of the interdecadal variability in the geopotential height over the SH mid- and high latitudes exhibits a zonal wavenumber-three structure along 60°S, with the major centers of action just upstream of the hemispheric land masses and substantial fluctuation in the strength of the tropospheric polar vortex.

We now investigate the seasonality of the SH circulation anomalies associated with interdecadal SST variability. In the right panels of Fig. 4, the seasonally averaged 500-hPa geopotential height is regressed upon GR. The anomaly pattern described for the austral winter (Fig. 4g) is even more pronounced during spring (Fig. 5h) and weakens in summer and autumn (Figs. 4e,f). The increase in the midtropospheric pressure gradient between Antarctica and midlatitudes associated with positive values of GR after 1977 implies a strengthened and more persistent tropospheric polar vortex during spring seasons after the late 1970s. This result is consistent with the decadal changes of the annual cycle of the pressure and winds at mid- and high latitudes in the SH presented by van Loon et al. (1993) and Hurrel and van Loon (1994) (e.g., Fig. 9 of Hurrel and van Loon 1994). Recently, it has been suggested that the reinforcement of the springtime polar vortex has occurred as a decadal-scale upward trend of its intensity rather than as a discrete shift (D. W. J. Thompson 1998, personal communication). In any case, it is clear that the pattern of interdecadal variability obtained from pro-

jecting GR on the relevant meteorological fields accounts for only a fraction of the long-term circulation fluctuations in mid- and high latitudes.

Evidence of interdecadal variability of the circulation over the southern Indian Ocean region during the austral summer has been presented by Allan et al. (1995) and Reason et al. (1996). These studies indicate decadal-scale fluctuations of the anticyclonic circulation, SST, and cloudiness, with extreme and opposite anomalies during the periods 1921–41 and 1963–83. Since their analyses are based on four 21-yr epochs (selected on the basis of the interdecadal variability of the Southern Oscillation index), which in general do not match the decadal fluctuations present in the GR time series, it is difficult to compare their findings with our regression analysis.

The surface wind anomalies regressed upon GR are shown in Fig. 5b. As in the interannual case, the midlatitude westerly winds across much of the Pacific are weakened in response to the anticyclonic anomaly farther south (for positive GR values, like the period from 1977 to 1993). Elsewhere around 45°S, the deepened low pressure over Antarctica tends to accelerate the circumpolar low-level flow, especially south of Australia and across the Drake Passage. The low-level (1000–850 hPa) temperature between 120°E and 140°W near Antarctica exhibits departures of nearly 1 K (std dev)$^{-1}$ of GR, consistent with the warm advection by the anomalous meridional flow (Fig. 3c). Since these temperature anomalies persisted for a long period of time, they may have a potentially large impact in the ice–sea dynamics in subpolar latitudes. Furthermore, the reanalysis data indicate that mean wintertime low-level air temperature over much of Antarctica and adjacent oceans in the more recent epoch (1977–93) is nearly 2 K higher than the mean from 1958 to 1976.

3. Discussion

Some of the SH midlatitude circulation anomalies associated with the interannual ENSO are different from those associated with the decadal ENSO-like variability. On the interannual timescale, the midlatitude circulation anomalies appear to be due to teleconnections from the tropical Pacific via planetary waves (see, e.g., Fig. 3 and references in section 2a). The ''decadal'' circulation anomalies appear to be more related to wave–mean flow interactions in the subpolar and polar regions (Figs. 3 and 4).

An analogous result holds for the circulation anomalies in the midlatitudes of the NH. Consistent with previous studies, ZWB found that the midlatitude anomalies associated with ENSO are mainly expressed in the extension of the subtropical jet, presumably through wave–mean flow interactions and the changes in the Hadley circulation in the eastern/central tropical Pacific. In contrast, the decadal ENSO-like variability is expressed by the classic PNA teleconnection pattern,

suggesting that the origins in the decadal variability are primarily in the tropical Pacific (see Fig. 13 of ZWB).

The spatial signatures of interannual (ENSO) and interdecadal (ENSO-like) variability extend well into high latitudes and, therefore, our results are relevant in interpreting climate fluctuations over Antarctica documented in previous works. Our regressions indicate that in the Bellingshausen Sea (between 70° and 100°W along Antarctica), warm ENSO conditions (positive CT*) and warm ENSO-like conditions (positive GR) cause southwesterly wind anomalies and negative SSTs in this region. By themselves, these wind anomalies should create lower surface temperatures by anomalous advection of cold air. However, one would also expect these wind anomalies to push the sea ice offshore, expanding (equatorward) the area that is covered by sea ice. Where ocean is replaced by sea ice, ocean-to-atmosphere heat flux will be severely reduced, further amplifying the cooling of the surface air during ENSO. Indeed, several studies have found an inverse relationship between sea ice coverage and air temperature in the Bellingshausen Sea region (see Jacobs and Comiso 1997, and references therein). South of 60°S and between 130° and 170°W (i.e., west of the anticyclone in the southeast Pacific in Fig. 3c), warm ENSO events force circulation anomalies that enhance anomalous advection of warm air into this region. We also expect that the sea ice should retreat during ENSO due to the anomalies in the surface wind stress (not shown, but see Fig. 2b) and the enhanced warm air advection. Further calculations (not shown) using the reanalysis data show that during ENSO this region receives greater precipitation through enhanced moisture convergence, contrary to the results presented in Cullather et al. (1996).

The pan-Pacific nature of the anomalies associated with both the ENSO and decadal ENSO-like variability suggests that both of these phenomena are rooted in the Tropics. However, because in both hemispheres the midlatitude circulation anomalies are different on the interannual and decadal timescales, we expect the pattern of the heating anomalies in the Tropics to be different for these two phenomena. Unfortunately, there are insufficient data to construct from observations the precipitation patterns associated with the time series in Fig. 1. Instead, we present the surface wind and convergence anomalies and the upper-level (300 hPa) moisture anomalies associated with ENSO (Fig. 6) and decadal ENSO-like variability (Fig. 7); maps are generated by regression of the time series in Fig. 1 on the NCEP–NCAR reanalysis data for all calendar months. In both cases, the regression maps for DJF and JJA (not shown) are similar to their respective annual maps, although the signature of tropical convection tends to be sharper during the boreal winter.

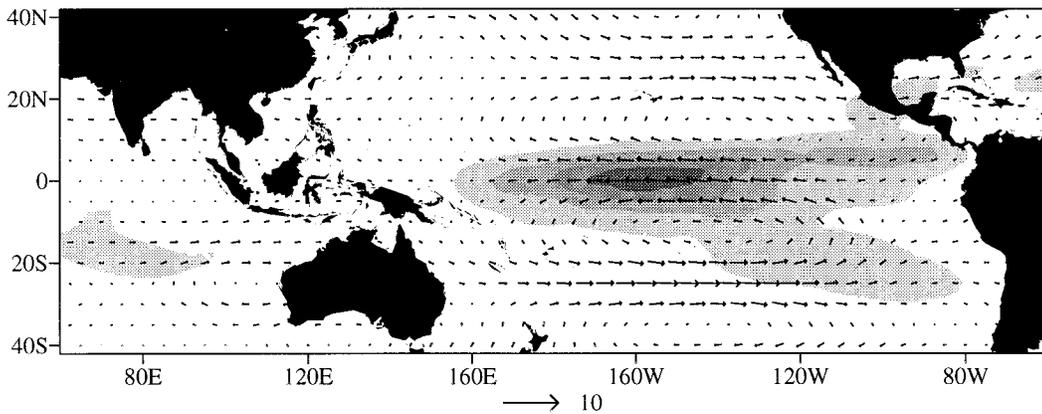As suggested by the moisture anomalies, and especially by the surface wind anomalies, the convective

< CT*, sfc. wind and sfc. wind divergence >
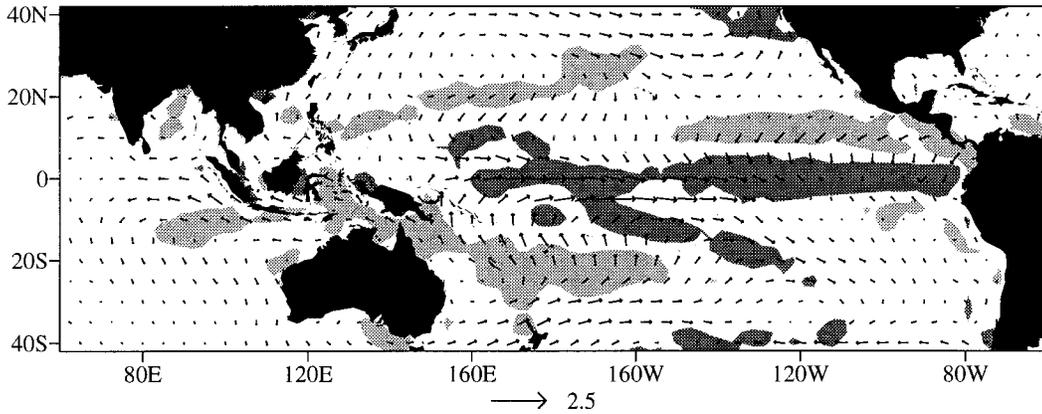
< CT*, 300 hPa winds and specific humidity >

FIG. 6. Global reanalyzed fields regressed upon CT* over the tropical Pacific. (top) Surface wind [the reference vector is 2.5 m s^{-1} (std dev)$^{-1}$] and surface wind divergence. Dark (light) shading indicates convergence (divergence) in excess of 0.25×10^{-6} s^{-1}. (bottom) 300-hPa winds [the reference vector is 7 m s^{-1} (std dev)$^{-1}$] and specific humidity. Light to dark shading indicates regression from 0.02 to 0.1 g kg^{-1} (std dev)$^{-1}$. Regressions are based on all calendar months from Jan 1958 to Dec 1993.

anomalies associated with the ENSO phenomenon indicate primarily a southward displacement of the ITCZ in the eastern and central equatorial Pacific, and an eastward displacement of the convection normally centered over the maritime continent, in agreement with the "observations" of tropical rainfall (based on outgoing longwave radiation and microwave sounding unit data) documented by Yulaeva and Wallace (1994). In contrast, the heating anomalies associated with the decadal ENSO-like variability highlight the northward displacement of the South Pacific convergence zone, with warm conditions in the tropical Pacific associated with positive anomalies in convection extending along a line from about 0°N, 170°E to 15°S, 130°W. In contrast to ENSO, there are no organized anomalies in precipitation in the eastern Pacific associated with the decadal variability.

The lack of such ITCZ signature is consistent with the broader SST anomalies in the eastern tropical Pacific on decadal timescales. We note that these results using the NCEP–NCAR reanalysis data are consistent with the precipitation anomalies that one would infer from the differences in the COADS wind stress anomalies associated with these two phenomena (cf., the middle panels of Figs. 11 and 12 in ZWB).[1]

---

[1] While COADS and the reanalysis data are consistent in the inferred location of the precipitation anomalies associated with GR, these two datasets show large differences in the GR-related winds in the far eastern, subtropical Pacific. These differences are not surprising, as the GR regressions using the COADS product shows a surface wind stress structure that is inconsistent with the SLP field,

< GR, sfc. wind and sfc. wind divergence >
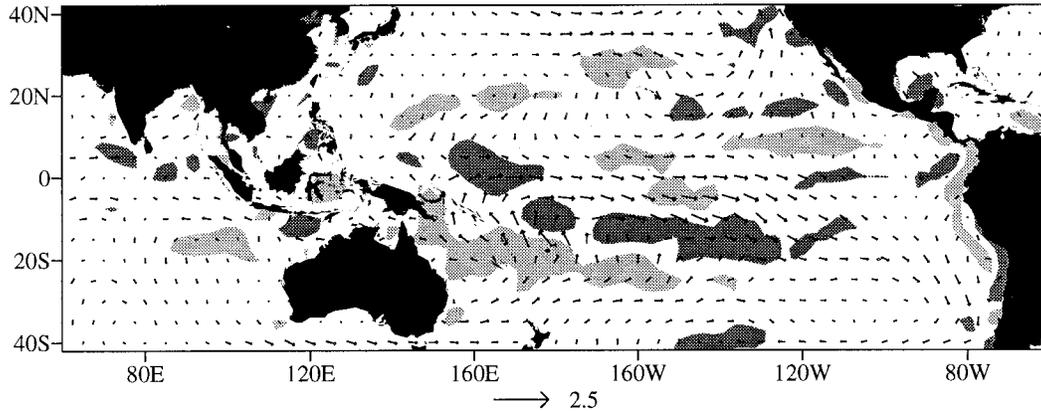
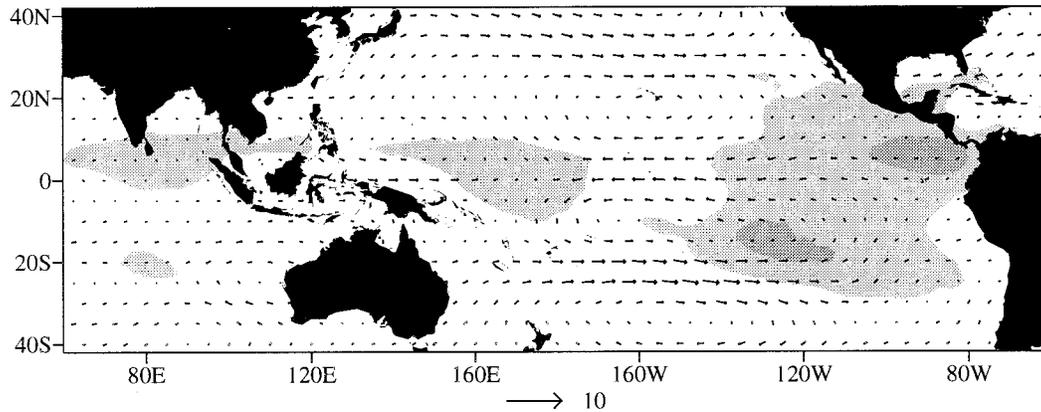< GR, 300 hPa winds and specific humidity >

FIG. 7. As in Fig. 6, but based on GR.

In summary, the pan-Pacific nature of the ENSO and decadal ENSO-like variability suggests that the origin for both of these phenomena is the tropical Pacific and that the midlatitude anomalies are *forced* from the Tropics. However, the differences between the pattern of the midlatitude circulation anomalies associated with the ENSO and the decadal ENSO-like phenomena suggests that different physical mechanisms must be at play in creating the midlatitude circulation anomalies on these two timescales. Consistent with this hypothesis, we have shown that within the tropical Pacific, there are notable differences between the patterns of the surface wind and upper-level moisture associated with the ENSO and decadal (ENSO-like) variability. It remains to be shown whether the implied differences between the precipita-

tion anomaly patterns (and, ultimately, the subtle differences between the SST anomaly patterns in the tropical Pacific) do indeed force the important differences in the midlatitude circulation anomalies associated with these two phenomena.

4. Concluding remarks

ZWB documented the circulation and SST anomalies associated with the ENSO and the decadal ENSO-like climate variability in the tropical and North Pacific Ocean and throughout the atmosphere in the Tropics and Northern Hemisphere. Zhang et al.'s analysis did not include the region south of 30°S. In this paper, we extended the work of ZWB to include the entire Southern Hemisphere, utilizing the data from the NCEP–NCAR reanalysis (1958–93). Our major findings include the following.

- Interannual and interdecadal variability exhibit similar

and that stress has a pattern that suggests it suffers from spatial interpolation (see Fig. 12b of ZWB).

spatial signatures in the SLP, low-level winds, and temperature fields over the Pacific Ocean in the Southern Hemisphere. Changes in the SST over the southern oceans appears to be forced by a local weakening or strengthening of surface heat flux due to changes in the atmospheric low-level circulation.

- However, the vertical structure of the interdecadal component over the Pacific is much different from that in the interannual case. In particular, the persistence and intensity of the PSA mode during the austral winter is strongly associated with the ENSO cycle, while it weakly projects onto decadal timescales. The spatial structure of the atmospheric circulation anomalies over the south Atlantic and Indian Oceans that are associated with ENSO and the decadal ENSO-like variability are similar, but the anomalies associated with the decadal variability tend to be much more marked in amplitude. Hence, interannual variability in the SH is associated with the PSA, whose physics implies teleconnection from the Tropics via Rossby wave propagation. In contrast, on decadal timescales the ENSO-like action in the tropical Pacific is expressed in the mid- and high latitudes in a different form, favoring a polar vortex and zonal wavenumber-three anomaly along 60°S.

- The anomalies in the surface wind convergence in the tropical Pacific that are associated with ENSO are significantly different from those associated with the decadal ENSO-like phenomenon. Further research is required to confirm that the inferred differences in the location of the tropical heating anomalies are responsible for the differences in the structure of the mid-latitude circulation anomalies associated with these different timescales of climate variability.

REFERENCES

Aceituno, P., 1988: On the functioning of the Southern Oscillation in the South American sector. Part I: Surface climate. *Mon. Wea. Rev.,* **116,** 505–524.

Allan, R. J., J. A. Lindesay, and C. J. C. Reason, 1995: Multidecadal variability in the climate system over the Indian Ocean region during the austral summer. *J. Climate.,* **8,** 1853–1873.

Cullather, R. I., D. H. Bromwich, and M.L. van Woert, 1996: Interannual variations in Antarctica precipitation related to El Niño–Southern Oscillation. *J. Geophys. Res.,* **101** (D14), 19 109–19 118.

Deser, C., and J. M. Wallace, 1990: Large-scale atmospheric circulation features of warm and cold episodes in the tropical Pacific. *J. Climate,* **3,** 1254–1281.

Fletcher, J. O., R. J. Slutz, and S. D. Woodruff, 1983: Toward a comprehensive ocean–atmosphere dataset. *Trop. Ocean–Atmos. Newsl.,* **20,** 13–14.

Folland, C. K., and D. E. Parker, 1995: Correction of instrumental biases in historical sea surface temperature data. *Quart. J. Roy. Meteor. Soc.,* **121,** 319–367.

Graham, N. E., 1994: Decadal-scale climate variability in the 1970s and 1980s: Observations and model results. *Climate Dyn.,* **10,** 135–162.

Horel, J. D., and J. M. Wallace, 1981: Planetary-scale atmospheric phenomena associated with the Southern Oscillation. *Mon. Wea. Rev.,* **109,** 813–829.

Hoskins, B. J., and D. J. Karoly, 1981: The steady linear response of a spherical atmosphere to thermal and orographic forcing. *J. Atmos. Sci.,* **38,** 1178–1196.

Hurrel, J. W., and H. van Loon, 1994: A modulation of the atmospheric annual cycle in the Southern Hemisphere. *Tellus,* **46A,** 325–338.

Jacobs, S. S., and J. C. Comiso, 1997: Climate variability in the Amundsen and Bellingshausen seas. *J. Climate,* **10,** 697–709.

Kalnay, E. M., and Coauthors, 1996: The NCEP/NCAR Reanalysis Project. *Bull. Amer. Meteor. Soc.,* **77,** 437–471.

Karoly, D. J., 1989: Southern Hemisphere circulation features associated with El Niño–Southern Oscillation. *J. Climate,* **2,** 1239–1252.

Kidson, J. W., 1988: Interannual variations in the Southern Hemisphere circulation. *J. Climate,* **1,** 1177–1198.

Kiladis, G. N., 1997: Interannual variability of the South Pacific circulation related to the Southern Oscillation. Harry van Loon Symp. Studies in Climate II, NCAR Tech. Note TN- 433+PROC, 300 pp. [Available from UCAR Communications, P.O. Box 3000, Boulder, CO 80307-3000.]

Mo, K. C., and M. Ghil, 1987: Statistics and dynamics of persistent anomalies. *J. Atmos. Sci.,* **44,** 877–901.

——, and R. W. Higgins, 1998: The Pacific South American modes and the tropical intraseasonal oscillation. *Mon. Wea. Rev.,* **126,** 1581–1596.

Nakamura, H., G. Lin, and T. Yamagata, 1997: Decadal climate variability in the North Pacific during the recent decades. *Bull. Amer. Meteor. Soc.,* **78,** 2215–2225.

Nitta, T., and S. Yamada, 1989: Recent warming of tropical sea surface temperature and its relationship to the Northern Hemisphere circulation. *J. Meteor. Soc. Japan,* **67,** 375–383.

Parker, D. E., C. K. Folland, A. C. Bevan, M. N. Ward, M. Jackson, and K. Maskell, 1995: Marine surface data for analysis of climatic fluctuations on interannual-to-century time scales. *Natural Climate Variability on Decade-to-Century Time Scales,* D.G. Martinson, Ed., National Academy Press, 123–152.

Reason, C. J. C., R.J. Allan, and J.A. Lindesay, 1996: Dynamical response of the oceanic circulation and temperature to interdecadal variability in the surface winds over the Indian Ocean region. *J. Climate,* **9,** 97–114.

Renwick, J. A., 1998. ENSO-related variability in the frequency of South Pacific blocking. *Mon. Wea. Rev.,* **126,** 3117–3123.

Reynolds, R. J., and T. M. Smith, 1994: Improved global sea surface temperature analyses using optimal interpolation. *J. Climate,* **7,** 929–948.

Rogers, J. C., and H. Van Loon, 1982: Spatial variability of sea level pressure and height anomalies over the Southern Hemisphere. *Mon. Wea. Rev.,* **110,** 1375–1392.

Ropelewski, C. F., and M. S. Halpert, 1996: Quantifying Southern Oscillation–Precipitation relationships. *J. Climate,* **9,** 1043–1059.

Rutllant, J., and H. Fuenzalida, 1991: Synoptic aspects of the central Chile rainfall variability associated with the Southern Oscillation. *Int. J. Climatol.,* **11,** 63–76.

Simmonds, I., and T. H. Jacka, 1995: Relationships between the interannual variability of Antarctic sea ice and the Southern Oscillation. *J. Climate.,* **8,** 637–647.

Sinclair, M. R., J. A. Renwick, and J. W. Kidson, 1997: Low-fre-

quency variability of Southern Hemisphere sea level pressure and weather system activity. *Mon. Wea. Rev.,* **127,** 2531–2542.

Trenberth, K. E., 1990: Recent observed interdecadal climate changes in the Northern Hemisphere. *Bull. Amer. Meteor. Soc.,* **71,** 988–993.

——, and J. W. Hurrel, 1994: Decadal atmosphere–ocean variations in the Pacific. *Climate Dyn.,* **9,** 303–319.

van Loon, H., and D. J. Shea, 1987: The Southern Oscillation. Part VI: Anomalies of sea level pressure on the Southern Hemisphere and of Pacific sea surface temperature during the development of a warm event. *Mon. Wea. Rev.,* **115,** 370–379.

——, J. W. Kidson, and A. B. Mullan, 1993: Decadal variations of the annual cycle in the Australian dataset. *J. Climate,* **6,** 1227–1231.

Wallace, J. M., and D. S. Gutzler, 1981: Teleconnections in the geopotential height field during the Northern Hemisphere winter. *Mon. Wea. Rev.,* **109,** 784–812.

——, E. M. Rasmusson, T. P. Mitchell, V. E. Kousky, E. S. Sarachik, and H. Storch, 1998: On the structure and evolution of ENSO-related climate variability in the tropical Pacific: Lessons from TOGA. *J. Geophys. Res.* **103** (C7), 14 241–14 259.

Yulaeva, E., and J. M. Wallace, 1994: The signature of ENSO in global temperature and precipitation fields derived from the microwave sounding unit. *J. Climate,* **7,** 1720–1736.

Zhang, Y., J. M. Wallace, and D. S. Battisti, 1997: ENSO-like interdecadal variability: 1900–93. *J. Climate,* **10,** 1004–1020.